INVESTIGATION ON THE NOISE OF AN AXIAL LOW MACH-NUMBER FAN STAGE WITH A HETEROGENEOUS STATOR

Miguel PESTANA[123], Marlène SANJOSÉ[2],
Stéphane MOREAU[2], Michel ROGER[3], Mathieu GRUBER[1]

[1] *Safran Aircraft Engines*
Rond-point René Ravaud, 77550 Moissy-Cramayel, France

[2] *Université de Sherbrooke*
2500 boul. de l'Université, J1K 2R1, Sherbrooke, Canada

[3] *Université de Lyon, LMFA, École Centrale de Lyon*
36 avenue Guy de Collongue, 69134 Écully, France

SUMMARY

A low-Mach number ducted axial fan from an aircraft air-conditioning system is investigated in this study. This configuration has a short rotor-stator distance and a heterogeneous (non-periodic) stator row. Those features strongly modify the rotor-stator noise-generation mechanisms. Two numerical simulations with the original heterogeneous and a homogeneous OGV are performed using the Lattice-Boltzmann Method (LBM). A comprehensive acoustic analysis is made upstream of the fan in order to retrieve the spectral and modal content of the noise. The direct comparison of the homogeneous and heterogeneous configurations provides the quantification of the impact of a heterogeneous stator. Finally, the dominant modes caused by the stator heterogeneity are identified by comparing with an experiment.

INTRODUCTION

This research focuses on several noise mechanisms in a single rotor-stator stage configuration at one operating condition. The configuration is a low-Mach number ducted axial fan, with several features of modern and future fan-OGV (Outlet-Guide-Vanes) architectures. Its blade-tip Mach number at full power is around 0.3, the high limit of the incompressible regime. Three stator vanes of the stage configuration are thicker for structural reasons. This heterogeneity is expected to regenerate duct modes that would not be exited in a homogeneous configuration as first evidenced by Roger & Caule [1] and more recently by Sanjosé *et al.* [2]. In a previous work, the configuration was experimentally investigated [3] and some dominant modes were also identified at the first three blade passing frequencies (BPF), whereas the first two should have been cut-off according to the Tyler & Sofrin's rule. The hub

to tip ratio (~ 0.5) and Helmholtz number (~ 15) based on the outer radius allow a significant modal content. Moreover, the short rotor-stator distance is expected to increase the contribution of the potential interaction noise emitted by the rotor, often neglected compared to the wake-interaction noise emitted by the stator. From a numerical standpoint, because of its low Mach number, the configuration allows performing computations with the Lattice-Boltzmann method (LBM) in its experienced domain of application.

The paper is organised as follows. The investigated configuration is first presented along with the numerical strategy. An aerodynamic investigation is then carried out. Finally, the simulation is investigated acoustically by means of in-duct spectra and modal content.

CONFIGURATION AND NUMERICAL STRATEGY

Experimental configuration

The present fan is a HVAC fan used in the cargo hold and galley cooling of aircraft. The configuration is installed in an experimental test facility at École Centrale de Lyon dedicated to accurate measurements. The duct is instrumented with both acoustic and aerodynamic sensors.

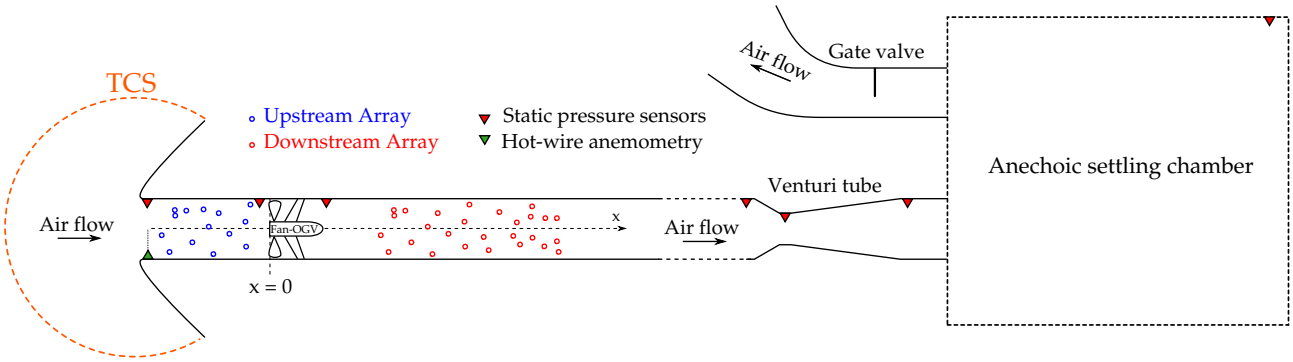

Figure 1: Sketch of the experimental setup in École Centrale de Lyon.

A sketch of the test facility is shown in Figure 1. The fan is made of $B = 17$ rotor blades and $V = 23$ stator vanes, three of which are thicker for structural needs, see Figure 2. A power-supply cable is also placed downstream of one of the heterogeneous stator vanes, see Figure 2(b). This cable may cause an additional potential distortion. The chords of the rotor blades and stator vanes are respectively $C_B = 2.1$ cm and $C_V = 3$ cm. The distance between the rotor blade trailing edge and the stator vane leading edge varies from $0.79C_B$ at the hub to $1.14C_B$ at the tip. The reduced rotor-stator distance makes some blade response to the downstream perturbations (interaction with the upstream potential field of the stator vanes) expected. The duct section is constant with a diameter of 170 mm.

The objective is to reproduce this experiment numerically by using the Lattice-Boltzmann Method.

Numerical strategy

The present simulations use the Powerflow solver 5.3b developed by Exa and based on the LBM. The approach is naturally transient and compressible, providing a direct insight into hydrodynamic mechanisms responsible for the acoustic emission but also into acoustic propagation.

Instead of studying macroscopic fluid quantities, the LBM tracks the time and space evolution on a lattice grid of a truncated particle distribution function. The particle distribution evolution is driven to the equilibrium by the so-called collision operator, approximated by the Bhatnagar-Gross-Krook model. The discretized Lattice-Boltzmann equations need to be solved for a finite number of particle

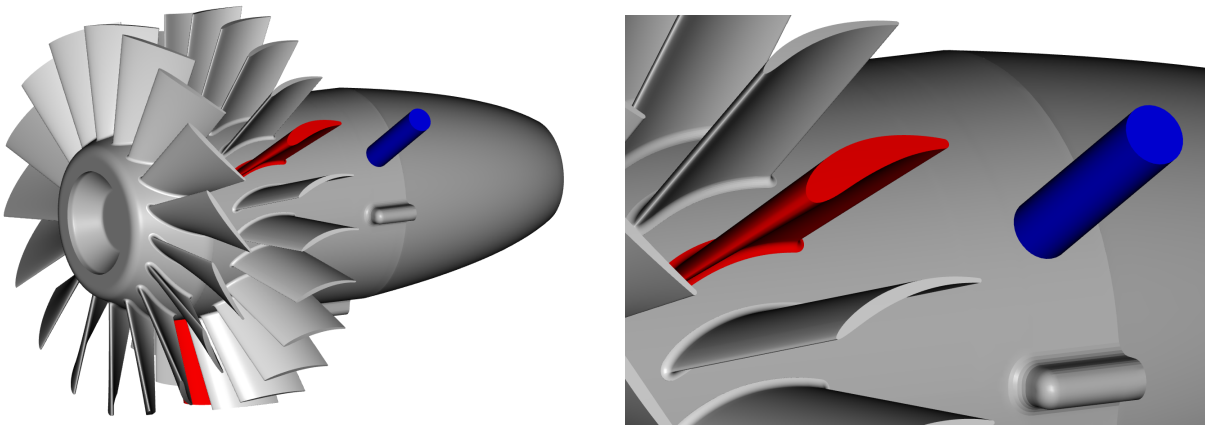

(a) Rotor-stator geometery. (b) Zoom on one modified stator vane.

Figure 2: Fan geometry. Courtesy of Safran Ventilation Systems.

velocities. The discretization retained in Powerflow involves 19 discrete velocities for the third order truncation of the particle distribution function, which has been shown sufficient to recover the Navier-Stokes equations for a perfect gas at low Mach number in isothermal conditions [4, 5, 6]. In Powerflow, a single relaxation time is used, related to the dimensionless laminar kinematic viscosity [7]. For large Reynolds-number flows, a Very Large Eddy Simulation mode is used in which the relaxation time is replaced by an effective turbulent relaxation time that is derived from a systematic Renormalization Group procedure detailed in Chen *et al.* [8]. It captures the large structures in the room (included in the computational domain) but also the small turbulent scales (resolved on the simulation grid) that develop along the blade and duct surfaces. At the wall, the shear stress is modeled by the use of a wall-law boundary condition accounting for pressure gradients and using specular reflections [9]. The particular extension of the method developed for rotating machines can be found in Zhang *et al.* [10].

Numerical setup

In order to accurately investigate the noise-generating mechanisms, the whole test facility at École Centrale de Lyon presented in the previous section is numerically simulated with some minor simplifications. The domain size is chosen according to the real room dimensions. However, the Venturi tube is replaced by a straight duct section and the ejection system removed (Figure 1). The experiments performed at École Centrale de Lyon have evidenced a negligible level of the reflected waves at the duct termination. For this reason, sponge zones are introduced in the duct in order to mimic the effect of the settling chamber. In addition to that, a sponge zone is added in the fluid domain far from the inlet in order to avoid unrealistic hard-wall reflections in the room. The air is re-introduced in the room through the whole back-wall referred to as 'Inlet' in Figure 3 showing the simulated domain.

The imposed outlet boundary condition is a uniform velocity profile in the duct cross-section in order to obtain the desired mass-flow rate. The mass-flow rate is not imposed directly at the outlet because it has acoustic reflective properties that would contaminate in-duct extractions. The inlet boundary condition sets a characteristic static pressure (measured atmospheric pressure in the experiments) along with free flow direction.

There are eight levels of refinement in the volume mesh reaching 0.3 mm of resolution at the rotor and stator walls for the finest cubic cell elements (or voxels). In terms of dimensionless wall distance, y_+ varies from around 30 at the blade hub to approximately 70 at the blade tip region where the shear is higher. For the stator, the average y_+ is equal to 45. The resolution upstream and downstream of the

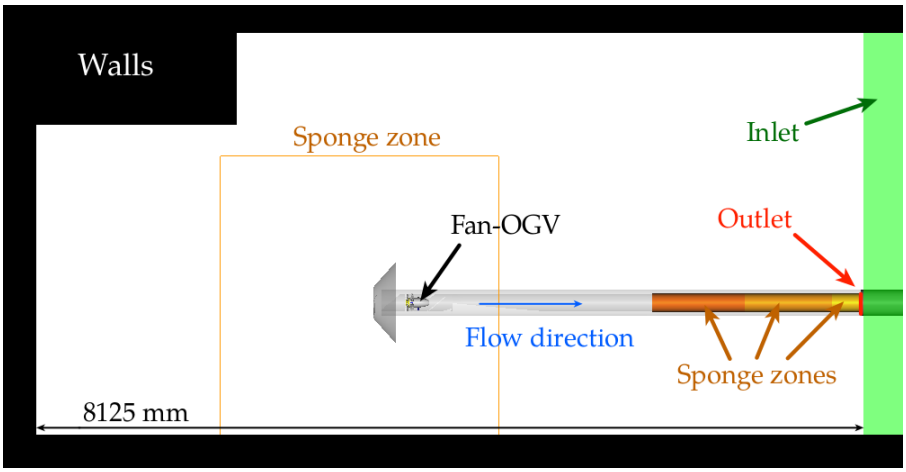

Figure 3: Simulation domain.

duct was defined to ensure a correct sound propagation up to the third blade passing frequency of the configuration.

In terms of fan-OGV geometry, two stator configurations are simulated. The first stator is the same as in the experiments and thus heterogeneous. In the second case, the three heterogeneous stator vanes are replaced by baseline vanes in order to retrieve a periodic stator.

The available extraction points corresponding to the measurement locations are shown in Figure 4. The same acoustic arrays as in the experiments are added for a better comparison (red probes shown upstream and downstream). Low frequency measurement disks for aerodynamic analyses are featured in blue. In addition to the disks, some thin hollow cylinders are added to investigate the flow topology in the rotor-stator region. In magenta are shown higher frequency extraction cross-sections in order to perform acoustic analyses such as modal decompositions. Finally, a cylinder dedicated to high frequency extraction including the whole rotor-stator configuration is added in order to perform detailed inter-stage analysis (contour shown in green).

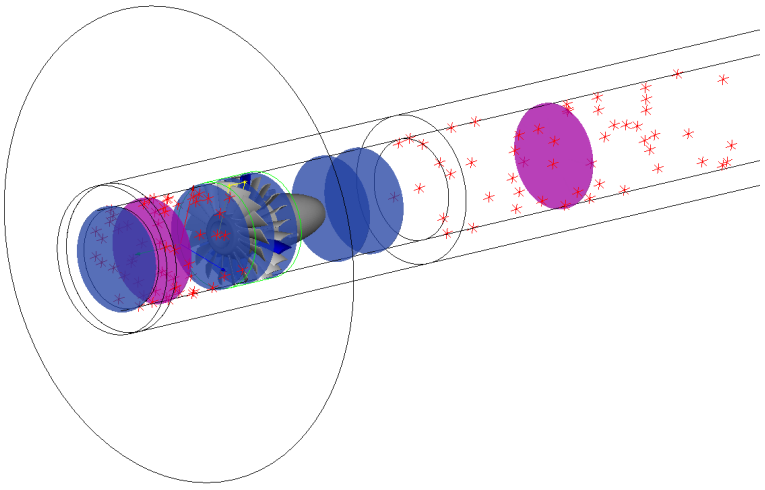

Figure 4: Numerical extractions for acoustic and aerodynamic analyses.

Table 1 defines the targeted experimental operating point of the present simulation. The condition corresponds to one of the nominal operating points according to the fan specifications data. The main simulation and measurement parameters are summarized in Table 2.

Rotational speed	Ω	10000 rpm
Mass flow rate	Q_m	0.8254 kg/s
Pressure jump	ΔP	1975.83 Pa
Atmospheric pressure	p_{atm}	98394 Pa

Table 1: Targeted experimental operating point.

Stator geometry		Case 1: heterogeneous (as in experiments) Case 2: homogeneous
Minimum voxel size	Δx	0.3 mm
Dimensionless wall distance	y^+	30 to 70 (hub to tip in the rotor)
	y^+_{max}	45 (in the stator)
Timestep	Δt	4.943×10^{-7} s
Mesh size	N_{voxels}	$\sim 50 \times 10^6$
Reynolds number	Re_D	978'310
Tip Mach number	M_{tip}	0.26
Sampling frequency:		
- *Aerodynamic measurement disks*	F_e	1000 Hz
- *Acoustic measurement disks and probes*	F_e	21075 Hz
- *Fine interstage measurement*	F_e	59510 Hz

Table 2: Simulation and measurement parameters.

AERODYNAMIC ANALYSIS

In this section, a detailed aerodynamic analysis is provided. In order to perform relevant investigations, it was ensured that the flow was stationary in terms of aerodynamic performance. The simulation initialized from rest has a transitional flow regime of about 20 revolutions after which performances are stabilized. The same behavior is observed for the homogeneous and heterogeneous stator cases. The experimental mass flow rate is correctly recovered with an error of about 0.5%. However, the pressure rise at the fan stage is lower by about 16%. For a better insight, the pressure evolution in the duct is shown in Figure 5 and compared with a RANS simulation performed by Sanjosé *et al.* [11].

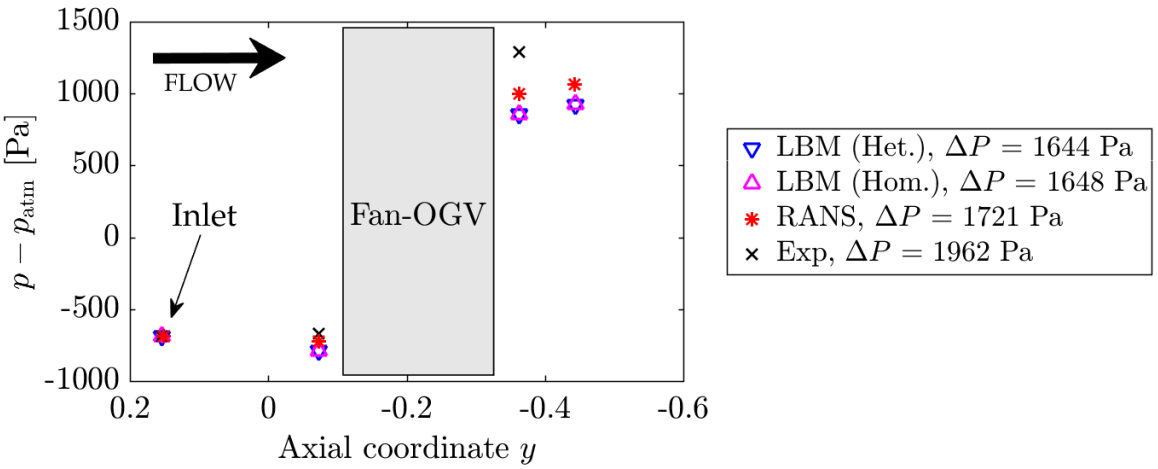

Figure 5: Pressure evolution in the duct. Comparison between numerical simulations and measurements.

The RANS simulation is performed on a reduced domain with three blades and four homogeneous stator vanes. The maximum y^+ equals 1.4 at the blades and 2 at the vanes surfaces. All numerical results

are shifted so that the pressure at the inlet is matched with the experiments. This allows comparing results in terms of relative variations.

The pressure rise from the RANS simulation is lower by 12% compared to the experiment but only higher by 4% compared to the LBM simulations. There is no clear explanation for those mismatches between numerical and experimental results. However, it is suspected that the pressure losses at the duct walls in the simulations are increased by the lower flow resolution in these regions. In fact, Figure 5 exhibits increased pressure losses from the inlet to upstream the fan compared to the experiments.

In terms of geometrical modification, the homogeneous stator geometry preserves the operating conditions of the fan.

As an additional validation, the LBM pressure coefficients on the rotor and stator are compared with the RANS results in Figure 6.

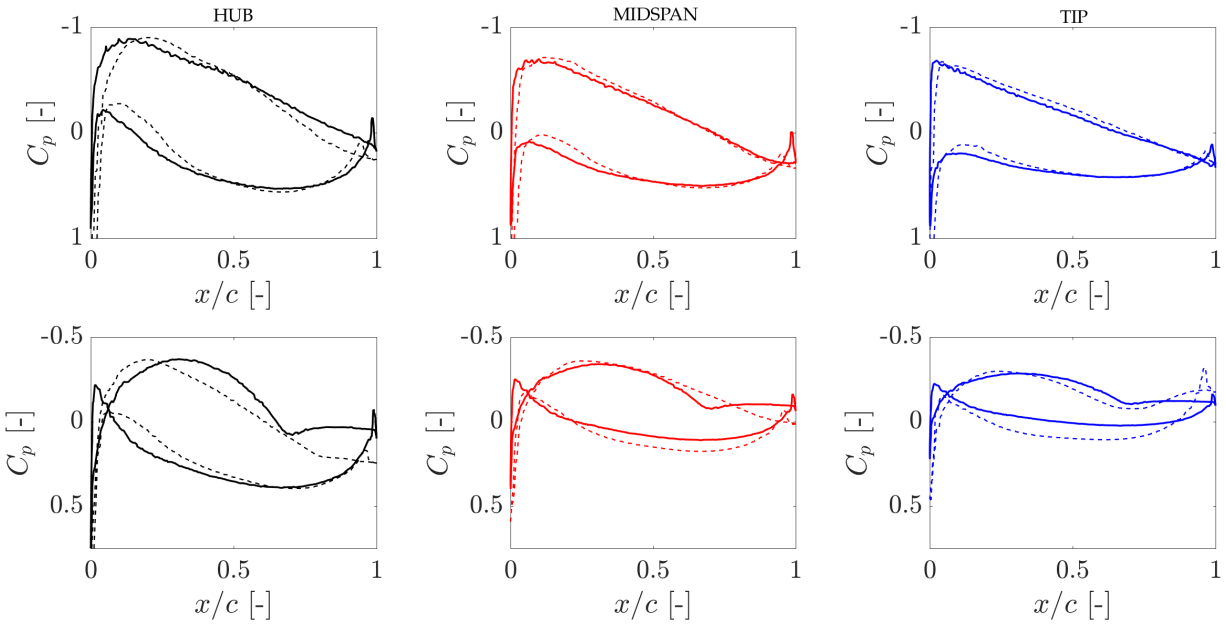

Figure 6: Mean pressure coefficients from the LBM (-) and RANS (- -) simulations for the hub (left), midspan (middle) and tip (right) regions. The upper plots are for a rotor blade and the lower plots for a homogeneous stator vane.

Both simulations agree well on the rotor, the biggest differences being observed closer to the hub. For the stator, a negative incidence in observed in the first 5% and a flow separation at around 70% of the vane chord. This flow separation is not as pronounced in the RANS simulations but has been observed in a previous study [3]. Flow separations can also be visualized from the instantaneous flow fields of the LBM at the hub, midpsan and tip in Figure 7. Moreover, the tip clearance is not accounted in the LBM as opposed to the RANS thus changing the flow topology at the tip between both simulations. Despite this, the general pressure-coefficient dynamics is correctly reproduced.

From the aforementioned comparisons it can be assessed that even having quite large y^+ in the LBM, the wall function allows correctly recovering the pressure distribution. The resolution of the mesh is high enough at the blade/vane surfaces to ensure a good aerodynamic prediction. Finally, the investigation of an upstream plane evidenced no inflow distortion.

Aerodynamic excitations

Two main sources are expected in this configuration: potential-interaction and wake-interaction. Both can be investigated by inspection of the aerodynamic excitations in the inter-stage. For that, phase-

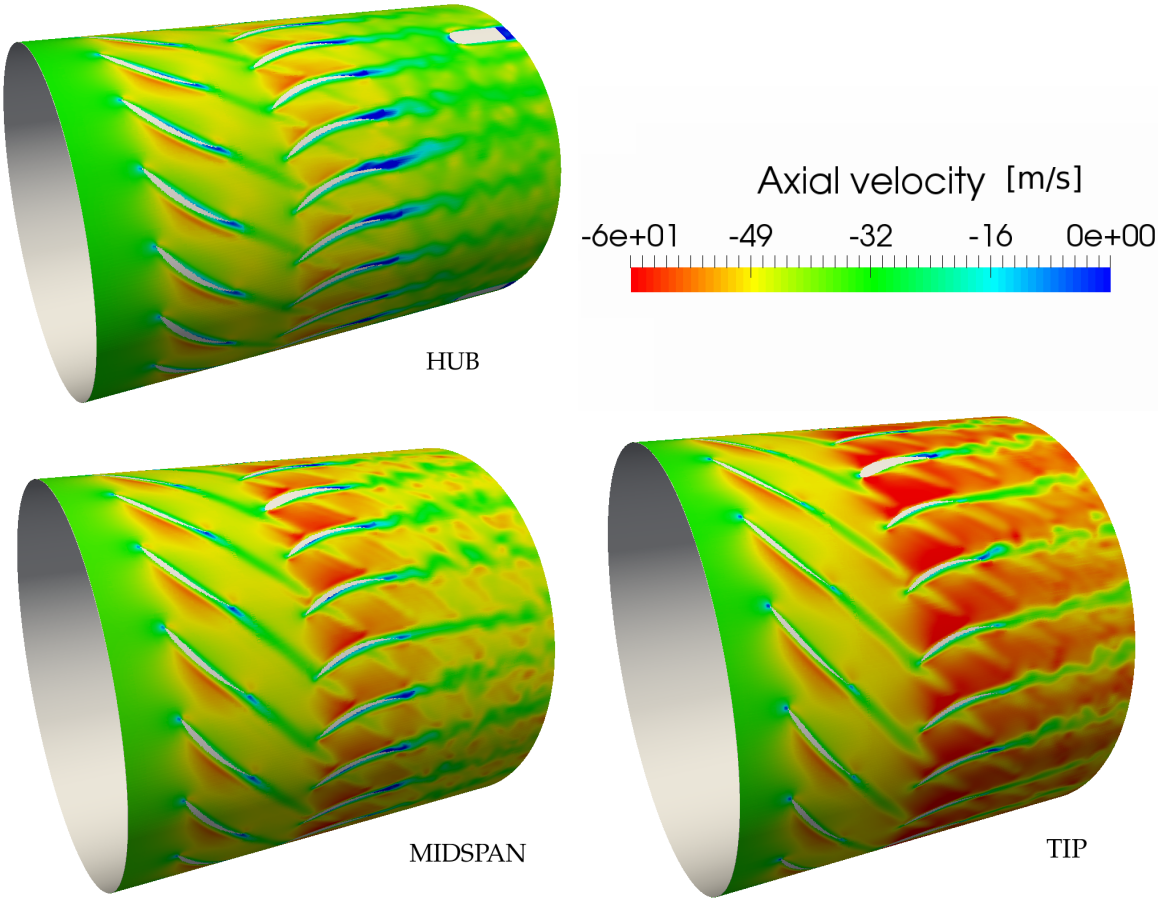

Figure 7: Instantaneous axial-velocity field at hub (upper-left), midspan (bottom-left) and tip (bottom-right).

averaging procedures allow to extract either the potential flow field upstream of the stator vanes or the wake flow field downstream of the rotor [2]. The potential field represents a downstream excitation for the rotor and is associated to the potential-interaction noise. The wake field produced by a rotor-locked average corresponds to the velocity perturbations at the origin of the so-called wake-interaction noise. This averaging procedure has been performed on a high-frequency extraction volume and during three revolutions. Because of lack of time, only the heterogeneous case could be recorded. The averaged fields are shown im Figure 8.

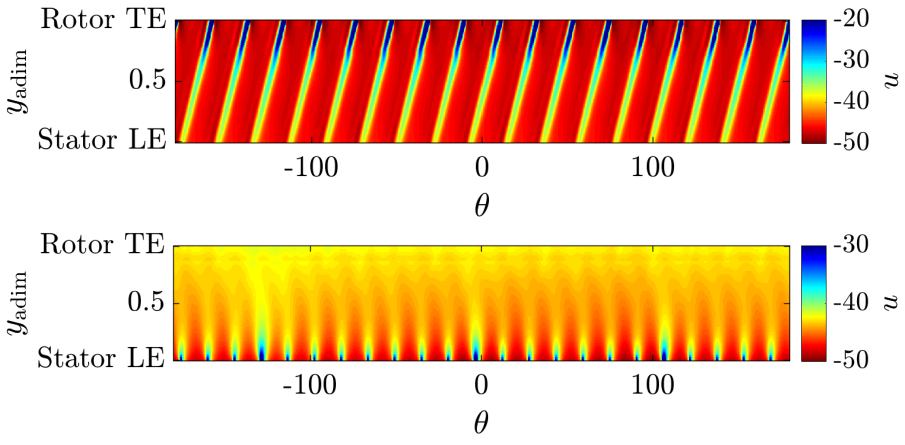

Figure 8: Phase-averaged axial velocity fields in the rotor (upper) and stator (lower) reference frames.

In the potential field, lower map,the influence of the three heterogeneous stator vanes is clearly identi-

fied. Three spots of lower axial velocity are observed in front these stator vanes. From these fields, an azimuthal Fourier analysis of the axial velocity is performed for each axial position in the interstage. The results are plotted in Figure 9.

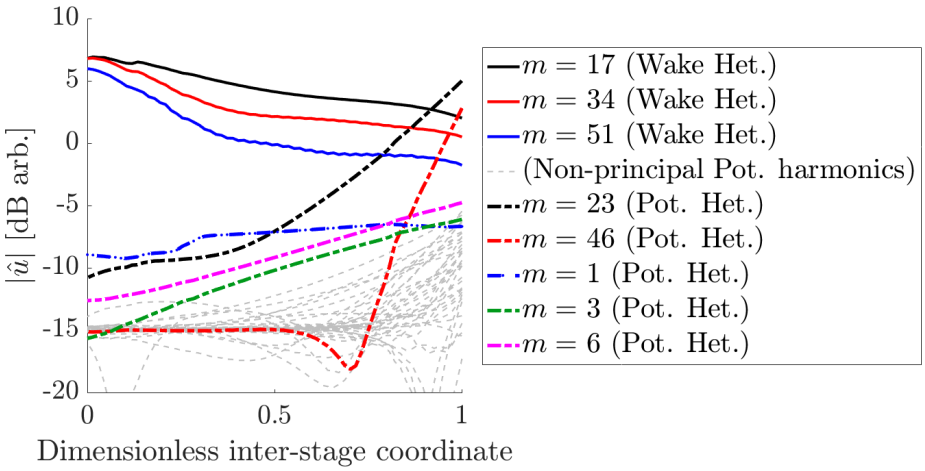

Figure 9: Spatial evolution of the azimuthal Fourier coefficients for the wake and potential fields for the heterogeneous case.

The main wake harmonics (multiples of the number of blades) are plotted along with the main potential harmonics (multiples of the number of vanes). The potential field is found to decrease rapidly, the decaying rate increasing with the harmonic order. This was also observed in a previous study [2]. By comparing both wake and potential, the potential harmonics seem to reach negligible levels at the rotor trailing edge whereas wake harmonics still have substantial level at the vane leading edge. It is therefore expected that the wake-interaction noise will contribute dominantly to the total rotor-stator interaction noise. However, this analysis was performed on the velocity field. As shown recently by Kozlov *et al.* [12], potential perturbations can be dominated by pressure. For this reason this source could have a higher contribution if investigated from pressure perturbations. Furthermore, because of the heterogeneity, other modes orders than nV are observed, mainly low orders. In fact, the mode order $n = 1$ is seen to be comparable to main harmonic $n = 23$ at the rotor trailing edge. This is a consequence of the stator heterogeneity which breaks the periodicity from vane to vane. In a perfectly periodic stator, those low-order modes would not be generated.

ACOUSTIC ANALYSIS

The available acoustic numerical extractions are post-processed in this section, essentially focusing on the BPF harmonics and corresponding modal contents.

In order to retrieve the modal content, two approaches are investigated. First, a simple azimuthal Fourier transform is performed. This approach has the advantage of determining azimuthal modes above the cut-off without any further consideration. The azimuthal content is expanded as:

$$p(x, r, \theta, \omega) = \sum_{m=-\infty}^{+\infty} p_m(x, r, \omega) \mathrm{e}^{\mathrm{i}m\theta} \tag{1}$$

However, a full modal decomposition is required to get access to the radial modal content. The pres-

sure at the duct section is then secondly expressed as follows:

$$p(x,r,\theta,\omega) = \sum_{m=-\infty}^{+\infty} \sum_{n=0}^{+\infty} \frac{f_{mn}(r)}{\Gamma_{mn}} \left[A_{mn}^{+} \mathrm{e}^{\mathrm{i}\gamma_{mn}^{+}x} + A_{mn}^{-} \mathrm{e}^{\mathrm{i}\gamma_{mn}^{-}x} \right] \mathrm{e}^{\mathrm{i}m\theta} \tag{2}$$

The summation is done over cut-on modes only. If cut-off modes are to be accounted for, it is necessary to define a position from which they decay exponentially. As shown in a previous work [3], this causes some difficulty. In the present case and at the considered rotational speed, it was verified that at the measurement positions cut-off modes have decreased enough so that they do not pollute probe measurements. The expansion relies on the assumption of an infinite duct of constant cross-section with a uniform axial flow. The axial flow velocity is obtained numerically by taking the average value of the velocity in the extraction plane where the modal decompositions are performed.

The radial shape functions proposed by Rienstra [13] are used here:

$$f_{mn}(r) = N_{mn} \left[\cos(\tau_{mn}) J_m(K_{mn} r) + \sin(\tau_{mn}) Y_m(K_{mn} r) \right] \tag{3}$$

The normalization factors N_{mn} and constants τ_{mn} can be found in [13]. The duct eigenvalues K_{mn} are only depend on the duct outer radius (cylindrical duct).

First, the spectra from wall-mounted duct microphones of the upstream array are investigated in Figure 10. The first two BPFs which should be cut-off according to the Tyler & Sofrin criterion are observed in both configurations. However, they are clearly increased in the heterogeneous configuration. The first BPF is increased by 10 dB and the second BPF by 13 dB compared to the homogeneous case. The third BPF level is kept almost constant. This is consistent with the clue that heterogeneity modifies more importantly the destructive interferences of cut-off BPFs but has probably a minor effect on cut-on BPFs. These results indicate that sound is not produced by classical rotor-stator interactions of homogeneous stages.

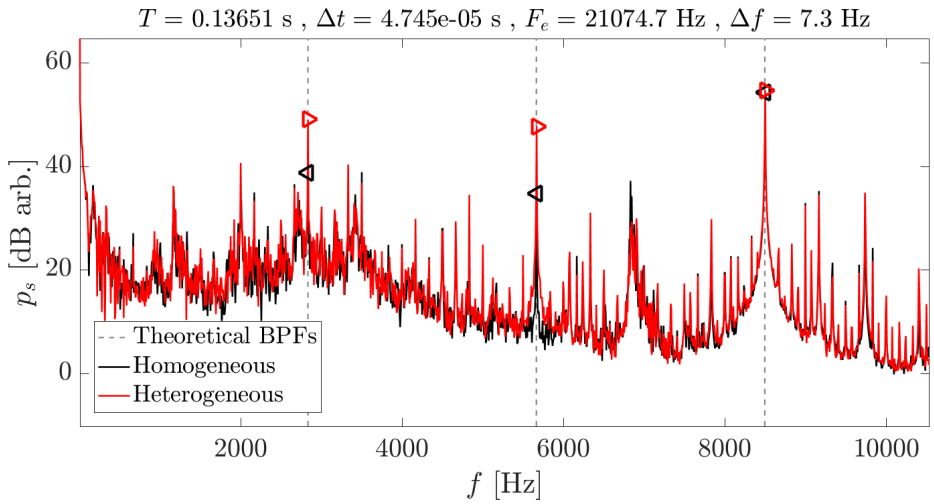

Figure 10: Averaged spectra from numerical probes of the upstream array for the homogeneous and heterogeneous simulations.

In the homogeneous case, the first two BPFs (black symbols in the figure) are still present. This may have two reasons. Firstly, the presence of a power-supply cable downstream the OGV introduces an additional potential distortion, similar to what has been investigated by Kozlov *et al.* [12]. Secondly, non-uniform rotor-wakes impinging the stator could also generate rotational shaft harmonics and thus also contribute at the BPFs.

It is worth noting that the post processing does not include the decontamination of the pseudo-sound pressure from the boundary layer fluctuations. However, apart from the BPF, tonal frequencies emerge, some of which are harmonics of the rotational frequency. For harmonics of the rotation to appear, the wakes of the blades impinging on the stator must not be periodic from blade to blade. Further investigation has to be carried out in order to conclude because in the present case rotor blades are identical.

The same conclusions can be derived from the results of the downstream array not shown here. Later on attention will be focused on the upstream measurements.

For a more detailed analysis, the azimuthal modal content over the radius is shown in Figure 11. For all BPF tones, the major modal content is concentrated close to the tip. At the first BPF in the heterogeneous case, the modes of order $m = -3$ and $m = 3$ are dominants. At the second BPF, the mode $m = 5$ is dominant. Finally, at the third BPF, the Tyler & Sofrin mode $m = 5$ is observed along with another non-expected mode $m = 11$. In the homogeneous case, the first two BPFs have low levels with no dominant modes. At the third BPF, only the Tyler & Sofrin mode is retrieved. This highlights the effect of the heterogeneous stator on the first two BPFs.

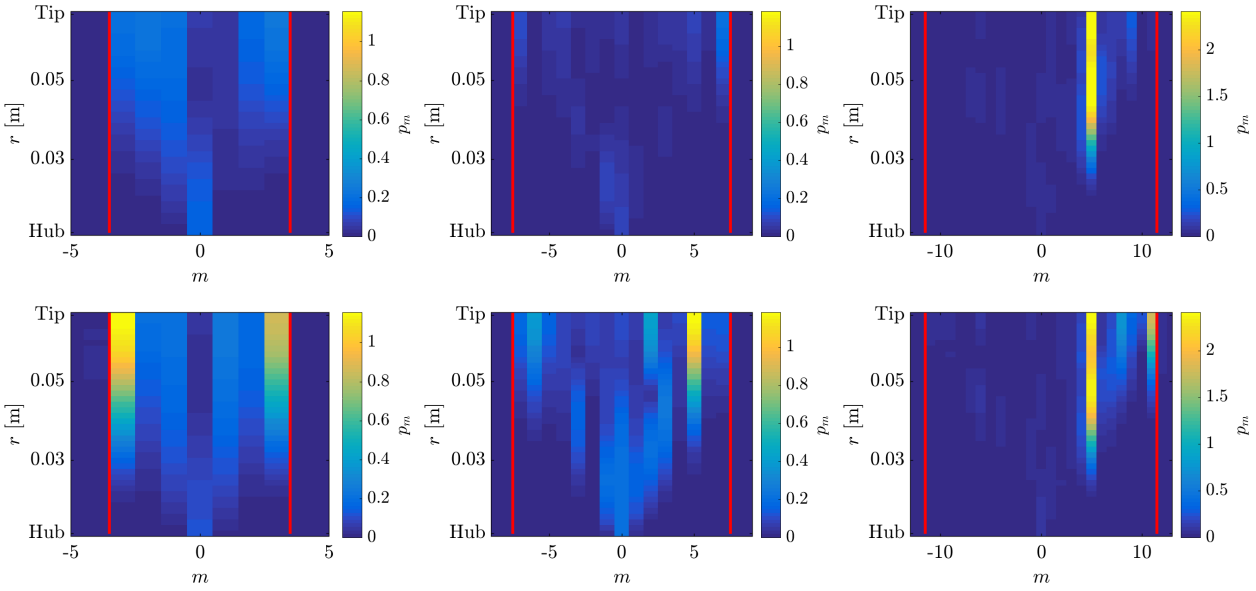

Figure 11: Radial evolution of the azimuthal modal content at the first three BPFs in one upstream plane. First row: homogeneous. Second row: heterogeneous. Left: first BPF. Center: second BPF. Right: third BPF. The red lines indicate limits of the cut-on range.

Full modal decompositions were also performed according to equation (2). Results are presented in Figure 12 for the first three BPFs and are compared to the measurements performed at École Centrale de Lyon [3]. The same modes as those identified from the azimuthal analysis are found. Most of the energy is here concentrated in the radial order $n = 0$. This is partly due to the fact that azimuthal dominating orders are cut-off for higher radial orders. In fact, it is observed that at the third BPF, the mode $m = 5$ spreads its energy on the first two radial orders.

In the experiment [3], nearly the same modes were observed at the same operating point except for the mode $m = 3$ at the first BPF. Some discrepancies in terms of mode amplitudes are also observed, mostly at the third BPF. However, the results are in a good agreement in terms of dominant modes. Again, it is confirmed that at the first two BPFs of the homogeneous case, no dominant mode can be identified. According to the comparison with the homogeneous and heterogeneous cases, the emergence of these modes at the first two BPFs can be attributed to the heterogeneity of the stator. The analytical prediction of these dominant azimuthal orders is still to be investigated. It is to note that the

heterogeneous stator-vanes are not equally distributed on azimuth (3 from 23) making this prediction exercise more difficult.

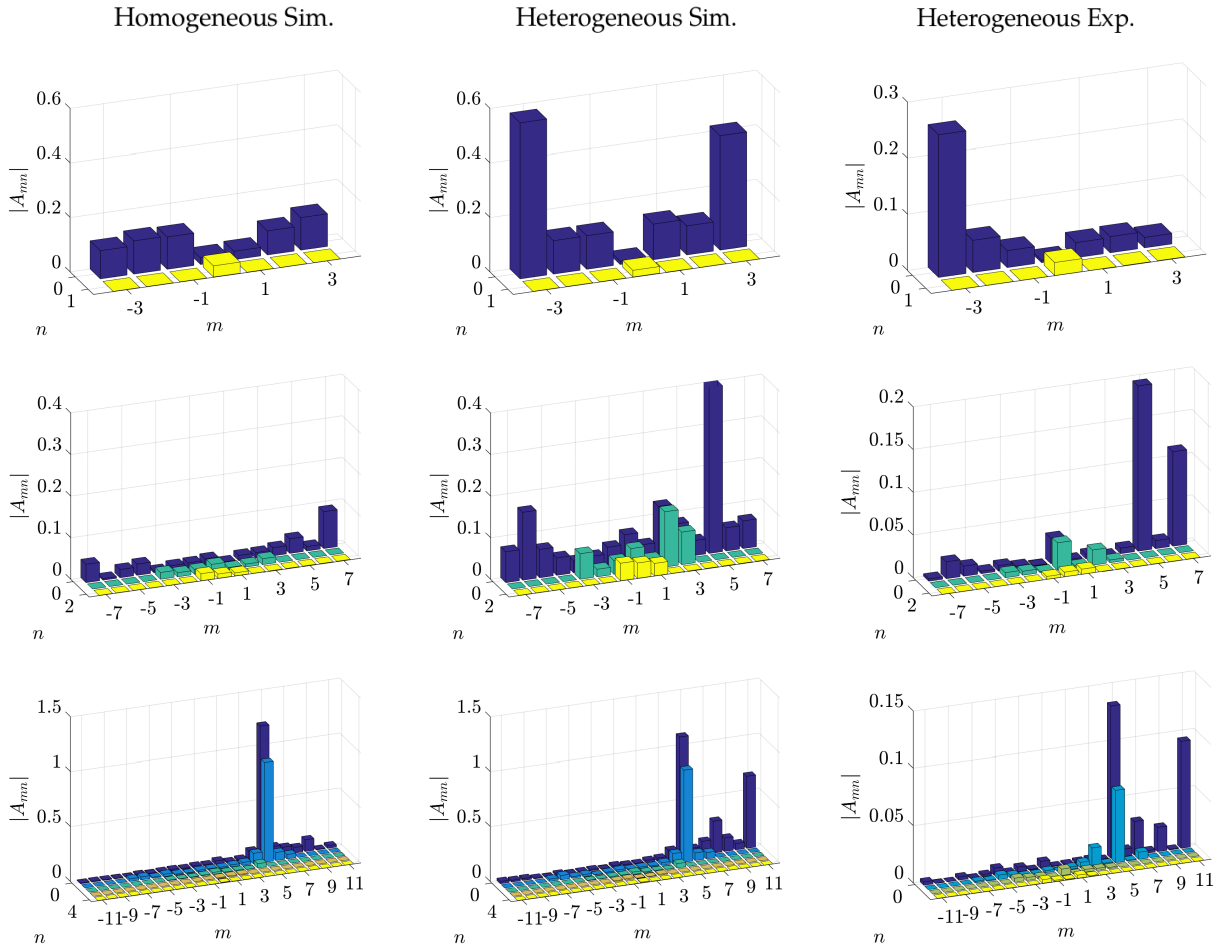

Figure 12: Modal content at the first three blade passing frequencies in one upstream plane. Left: homogeneous simulation. Center: heterogeneous simulation. Right: heterogeneous experimental configuration. First line: first BPF. Second line: second BPF. Third line: third BPF.

CONCLUSION

In this paper, a low-speed aircraft air-conditioning fan was numerically investigated with a LBM solver. In terms of aerodynamic performances, the simulation produced a lower pressure rise compared to the experiments. However, the results are in agreement with RANS simulations of the same configuration. Higher pressure losses in the simulations due to the mesh resolution at the duct may explain the deviation from the experiments. In terms of acoustics, a strong effect of the stator heterogeneity was shown. An increase of more than 10 dB is predicted at the first two BPFs in comparison with the homogeneous case. These first two blade-passing frequencies should be cut-off according to the Tyler & Sofrin criterion. Finally, by looking at the modal content at such frequencies, dominating modes could be identified. These mode were observed to be identical to the measured ones in the same configuration. In terms of source contribution, the first analysis concludes that potential-interaction noise is negligible compared to wake-interaction noise in spite of the short rotor-stator distance. The heterogeneity is shown to be the cause of a significant increase in the noise levels. It is responsible for the excitation dominant modes at BPFs which should be cut-off in a perfectly periodic stator.

REFERENCES

[1] M. Roger and P. Caule. *Assessement of the Effect of Stator Inhomogeneity on Rotor-Stator Tonal Noise*. In *ISROMAC-15*, **2014**.

[2] M. Sanjosé, S. Moreau, M. Pestana, and M. Roger. *Effect of Weak Outlet-Guide-Vane Heterogeneity on Rotor–Stator Tonal Noise*. AIAA Journal, pages 1–18, **2017**.

[3] M. Pestana, A. Pereira, E. Salze, J. Thisse, M. Sanjosé, E. Jondeau, P. Souchotte, M. Roger, S. Moreau, J. Regnard, and M. Gruber. *Aeroacoustics of an axial ducted low Mach-number stage: numerical and experimental investigation*. In *23rd AIAA/CEAS Aeroacoustics Conference*, page 3215, **2017**.

[4] U. Frisch, D. D'Humiéres, B. Hasslacher, P. Lallemend, Y. Pomeau, and J-P. Rivet. *Lattice gas hydrodynamics in two and three dimensions*. Complex Syst., 1:649–707, **1987**.

[5] S. Chen and G. D. Dooler. *Lattice Boltzmann method for fluid flows*. Ann. Rev. Fluid Mech., 30:329–364, **1998**.

[6] S. Marié, D. Ricot, and P. Sagaut. *Comparison between lattice Boltzmann method and Navier-Stokes high order schemes for computational aeroacoustics*. J. Comp. Phys., 228:1056–1070, **2009**.

[7] E. Vergnault, O. Malaspinas, and P. Sagaut. *A lattice Boltzmann method for nonlinear disturbances around an arbitrary base flow*. J. Comput. Phys., 231:8070–8082, **2012**.

[8] H. Chen, S. A. Orszag, I. Staroselsky, and S. Succi. *Expanded analogy between Boltzmann kinetic theory of fluids and turbulence*. J. Fluid Mech., 519:301–314, November **2004**.

[9] H. Chen, C. Teixeira, and K. Molvig. *Realization of Fluid Boundary Conditions via Discrete Boltzmann Dynamics*. International Journal of Modern Physics C, 09(08):1281–1292, **1998**.

[10] R. Zhang, C. Sun, Y. Li, R. Satti, R. Shock, J. Hoch, and H. Chen. *Lattice Boltzmann Approach for Local Reference Frames*. Commun. Comput. Phys., 9(5):1193–1205, **2011**.

[11] M. Sanjosé, M. Pestana, S. Moreau, and P. Caule. *Evaluation of analytical aeroacoustic models for a low-speed axial ventilation system*. In *Fan 2018, Paper 106*, **2018**.

[12] A. V. Kozlov, H. M. Atassi, A. A. Ali, and D. A. Topol. *Modelling Fan Noise Produced by Downstream Mounting Structural Blockage*. In *23rd AIAA/CEAS Aeroacoustics Conference*, page 3871, **2017**.

[13] S.W. Rienstra and A. Hirschberg. *An Introduction to Acoustics*. Eindhoven University of Technology, **2004**.

ACKNOWLEDGEMENTS

The authors thank Université de Lyon for providing the necessary computational resources and for the technical support. The authors also acknowledge Damiano Casalino and Ignacio Gonzalez-Martino from Exa for the help in setting-up the simulation. This work was performed within the framework of industrial Chair ADOPSYS co-financed by Safran Aircraft Engines and the ANR (ANR-13-CHIN-0001-01) and is also supported by the Labex CeLyA of the Université de Lyon, within the programme 'Investissements d'Avenir' (ANR-10-LABX-0060/ANR-11-IDEX-0007) operated by the French National Research Agency (ANR).